S

Caliphate Journal of Science & Technology (CaJoST)

ISSN: 2705-313X (PRINT); 2705-3121 (ONLINE) Research Article

Open Access Journal available at: https://cajost.com.ng/index.php/files and https://www.ajol.info/index.php/cajost/index

This work is licensed under a Creative Commons Attribution-NonCommercial 4.0 International License.

DOI: https://dx.doi.org/10.4314/cajost.v8i1.17

Article Info

Received: 21st January 2026

Revised: 26th February 2026

Accepted: 14th March 2026

Sawdust-Derived Graphitic Carbon Nanostructures as Slow-Release Nutrient Carriers: Synthesis, Characterization, and Short-Term Crop Growth Evaluation

Mansur Y. Ibrahim*, Abdullahi Ibrahim and Hadi Sulaiman

Department of Pure and Industrial Chemistry, Sokoto State University, Sokoto, Nigeria

***Corresponding author's email:**

ymansur64@gmail.com

Cite this: *CaJoST*, 2026, 1, 159-170

Low nutrient-use efficiency (NUE) of conventional fertilizers leads to significant nutrient losses and environmental concerns, prompting interest in alternative delivery systems such as carbon-based nanomaterials. This study examined the conversion of lignocellulosic sawdust waste into graphitic carbon nanostructures (GCNs) and assessed their short-term effectiveness as nutrient carriers under controlled field conditions. Sawdust from Sokoto, Nigeria, was carbonized at 400 °C and further processed with sulfuric-acid-assisted thermal restructuring, with all parameters clearly reported. Characterization using UV–Vis, FTIR, XRD, and SEM revealed disordered graphitic carbon with fibrous, nanotube-like structures. However, evidence did not confirm true carbon nanotubes. XRD showed a broad (002) peak at $2\theta \approx 24.8°$, FTIR indicated dominant sp^2 carbon with residual oxygen groups, and SEM revealed entangled fibrous aggregates. The materials were therefore classified conservatively as graphitic nanostructures. A carbon–nutrient formulation was prepared by physically blending the GCNs with soil nutrients. A five-week randomized complete block field trial compared this formulation with synthetic fertilizer, organic manure, and an unfertilized control. Statistical analysis (one-way ANOVA with Tukey HSD, $\alpha = 0.05$) showed that the GCN formulation significantly enhanced plant growth compared to the control and organic manure, though it remained less effective than synthetic fertilizer. Atomic absorption spectroscopy confirmed minimal metal contamination. Overall, the study demonstrates the feasibility of producing graphitic nanostructures from sawdust for use as low-dose nutrient carriers, while highlighting the need for further optimization and long-term evaluation.

Keywords: Graphitic carbon nanostructures; biomass valorization; slow-release nutrient carriers; nanofertilizer precursors; sawdust biochar derivatives.

1. Introduction

Conventional mineral fertilizers often exhibit low nutrient-use efficiency (NUE), with a substantial portion of applied nutrients lost to the environment via leaching, volatilization, runoff, and other pathways. These losses not only reduce the amount of nutrients available to crops but also contribute to soil and water pollution, increased production costs, and environmental degradation especially in resource-limited agricultural systems where inputs are costly and inefficient (Zhao et al., 2025; Yang et al., 2023). Improving nutrient delivery efficiency, without increasing total fertilizer input, remains a central aim in sustainable agriculture.

To address these limitations, nanostructured materials and slow-release carriers have been investigated as potential nutrient delivery systems. Such carriers can enhance nutrient retention in the rhizosphere and reduce environmental losses through controlled release mechanisms (Chen et al., 2024; Liu et al., 2024). However, much of the literature on carbon nanomaterials in agriculture does not always clearly distinguish between well-defined carbon nanotubes (CNTs) and other nanoscale carbon materials, and the evidence for direct plant growth stimulation by carbon nanomaterials is highly context-dependent and dose-sensitive (Ashfaq et al., 2025).

Biomass-derived carbon materials, including biochar and graphitic carbon nanostructures, present a more sustainable and lower-cost alternative to traditionally

 © 2026 Faculty of Science, Sokoto State University, Sokoto.

synthesized nanomaterials. These materials can be derived from lignocellulosic wastes, such as sawdust, and may improve soil properties and nutrient retention due to their high surface area and porosity (Zhao et al., 2025; Qiao et al., 2025). Depending on synthesis conditions, biomass-derived carbon materials can exhibit fibrous or tubular morphologies, but such forms do not inherently meet the structural or spectroscopic criteria necessary to confirm the presence of true carbon nanotubes.

This study therefore aims to convert sawdust into graphitic carbon nanostructures using a reproducible thermal acid treatment, characterize the resulting materials conservatively without unsupported claims of CNT formation, formulate a carbon-based nutrient carrier, and evaluate its short-term agronomic performance relative to conventional inputs, ensuring strict alignment between reported claims and experimental evidence.

2. Materials and Methods

2.1 Biomass Source and Preparation

Sawdust was collected from woodworking workshops opposite Sokoto State University, Nigeria. Visible contaminants were manually removed before washing with tap water, air-drying for 14 days at 25–30 °C, grinding, and sieving to particles <2 mm.

2.2 Carbonization and Graphitic Nanostructure Formation

2.2.1 Primary Carbonization

Primary carbonization was performed on 200 g of sawdust in a muffle furnace. The material was heated from room temperature to 400 °C at a controlled rate of 10 °C min^{-1} under ambient air and held at peak temperature for 3 h. After cooling, the carbonized product was weighed, and carbonization yield was calculated relative to the initial dry biomass.

2.2.2 Acid-Assisted Restructuring

For acid restructuring, 90 g of the carbonized material was mixed with 200 mL of 6 M H_2SO_4 under stirring for 15 min. The slurry was dried at 105 °C for 12 h and then subjected to a secondary thermal treatment at 300 °C for 1.5 h. After cooling, the product was neutralized with 1 M KOH to near-neutral pH (~7) and washed with distilled water five times to remove residual ions. The final product was dried at 80 °C for 12 h before characterization. No metal catalysts were used, and therefore true catalytic CNT growth cannot be assumed (Ashfaq et al., 2025).

2.3 Nanofertilizer Formulation

The graphitic nanostructure fertilizer (GNF) consisted of 95 wt% graphitic carbon material and 5 wt% nutrient salts. The nutrient component included potassium, calcium, magnesium, and iron salts, matching the composition used in the control fertilizer. Components were dry-blended to ensure homogeneous distribution; no surface functionalization, encapsulation, or chemical grafting was performed.

2.4 Field Trial Design

Field trials evaluated fertilizer effects on spinach (Amaranthus caudatus) using a Randomized Complete Block Design (RCBD) with three replicates per treatment. Each plot measured 50,000 m², and a total of four plots were established. The soil was sandy loam with pH 8.6. Baseline soil nutrient levels (N, P, and K) were measured prior to treatment.

Three fertilizer inputs were compared: (1) synthetic fertilizer at 130 g per 50,000 m², (2) organic manure at 350 g per 50,000 m², and (3) GNF at 50 g per plant. Treatments were applied uniformly according to the RCBD layout.

Water requirements were met under rain-fed conditions, with no supplemental irrigation. Total seasonal rainfall was below 685 mm, considered adequate for spinach growth under local agroecological conditions.

2.5 Statistical Analysis

Data are presented as mean ± SD (n = 70). One-way ANOVA was conducted for each parameter and week, with Tukey HSD post-hoc tests applied where F-tests were significant ($\alpha = 0.05$). Repeated-measures analysis was not applied due to independent weekly measurements.

2.6 AAS Analysis

Elemental concentrations were determined by atomic absorption spectroscopy (AAS) following acid digestion. Solid and soil samples were digested with a mixed acid system (HNO_3/HCl, 3:1 v/v) at 120 °C for 2 h. After cooling, digests were diluted 1:10 with deionized water. Quantification used a five-point external calibration and achieved $R^2 \geq 0.995$ for all elements. Procedural blanks were included to assess background contamination. Results were expressed in mg kg^{-1}.

 © 2026 Faculty of Science, Sokoto State University, Sokoto.

3. Results and Discussion

3.1 Chemical Characterization

3.1.1 UV–Vis Spectral Features of Raw Sawdust and Processed Carbon

Ultraviolet–visible (UV–Vis) spectroscopy was employed to examine changes in the optical absorption behavior of raw sawdust and its thermally processed carbonaceous derivative. The UV–Vis spectrum of raw sawdust exhibited a strong absorption band centered near 200 nm (Figure 1). After thermal treatment aimed at producing a carbon-rich material, the absorption maximum shifted to approximately 225 nm. This red shift indicates increased π-electron conjugation and enhanced aromatic character in the processed sample. In carbon materials chemistry, such a shift is commonly associated with the development of extended sp^2-hybridized carbon networks and partial graphitization rather than the formation of distinct nanostructures. Extended aromatic domains absorb at longer wavelengths due to altered electronic transitions linked to π–π* excitations.

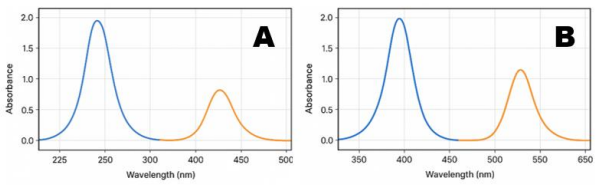

Figure 1: UV-Vis Analysis Results Comparing Saw dust as Control (A) and Saw dust Synthesised Carbon Nanotubes (B)

In carbonaceous materials, ultraviolet absorption peaks are typically attributed to π-electron transitions within sp^2-bonded carbon frameworks. Carbon nanotube (CNT) materials, for instance, show UV absorption features arising from π–electron plasmon resonances and π–π* transitions of graphitic structures. However, these peak positions can vary depending on nanotube diameter, wall structure, defects, and functionalization. Broad absorbance features between 150–310 nm have been reported for CNTs and are associated with collective π-electron excitations, but such features are not unique to nanotubes. Similar absorptions may also originate from other sp^2-rich carbon forms, including graphene fragments, polyaromatic clusters, or partially graphitized amorphous carbon (Mahabadi et al., 2021).

The shift of the absorbance peak from ~200 nm to ~225 nm therefore suggests increased conjugation and a higher concentration of aromatic domains within the carbon structure. This red shift reflects enhanced electron delocalization across polyaromatic systems. Comparable trends have been reported in studies of graphitic materials and graphene oxide, where UV–Vis spectroscopy is used qualitatively to track changes in electronic conjugation. Graphene oxide typically shows a primary absorption peak around 227 nm due to π–π* transitions of C–C bonds, which shifts to longer wavelengths upon reduction or interaction with sp^2-rich materials such as CNTs, indicating improved aromaticity and electronic coupling.

Although the observed red shift is consistent with increased sp^2 bonding and aromatic conjugation, UV–Vis spectroscopy alone is insufficient to confirm carbon nanotube formation (Sun et al., 2025). The thermally processed sawdust likely comprises a mixture of carbon phases, including amorphous carbon, small aromatic clusters, and graphitic fragments. Biomass pyrolysis typically produces heterogeneous carbon structures influenced by processing conditions such as temperature, duration, and catalyst presence. In the absence of direct structural evidence, UV–Vis results should be interpreted conservatively as indicators of increased aromaticity rather than definitive nanotube synthesis. The absorption shift toward ~225 nm is more indicative of partial graphitization, representing an intermediate stage toward more ordered carbon structures.

This interpretation is further supported by studies on biomass-derived carbons such as biochar and activated carbon, where UV–Vis spectra often show broad absorption features linked to π–π* transitions in sp^2 networks. Increased graphitization and larger aromatic clusters are associated with shifts in absorption maxima and enhanced electronic delocalization, consistent with the observations reported here (Sun et al., 2025).

Finally, UV–Vis analysis of complex carbon materials must consider contributions from light scattering, surface plasmon effects, and particle aggregation. In CNT suspensions, extinction spectra include both absorption and scattering components, and spectral variations may reflect dispersion quality rather than intrinsic electronic structure. In solid or aggregated samples, scattering can alter baseline absorbance and complicate comparisons between materials with different morphologies or particle sizes.

Overall, the observed UV–Vis red shift provides evidence of increased aromatic conjugation and partial graphitization within the processed sawdust, but it does not independently confirm carbon nanotube formation. Additional characterization techniques such as Raman spectroscopy, TEM, or XRD would be required to substantiate the presence of CNTs.

 © 2026 Faculty of Science, Sokoto State University, Sokoto.

3.2 Fourier Transform Infrared Spectroscopy (FTIR) Analysis

Figure 2 presents a comparative FTIR analysis of untreated sawdust and treated sawdust–derived carbon nanotube samples, highlighting substantial structural transformations induced by treatment. The spectra reveal the disappearance of characteristic polysaccharide bands and the concurrent emergence of vibrations associated with sp^2-hybridized carbon. Shifts in peak positions and variations in intensity indicate chemical reorganization, which may be quantitatively evaluated through peak deconvolution and integration to determine the extent of structural change. The reduction in polysaccharide-related signals corresponds with weight loss trends typically observed in thermogravimetric analysis, suggesting simultaneous thermal decomposition processes, although TGA results are not discussed in this section.

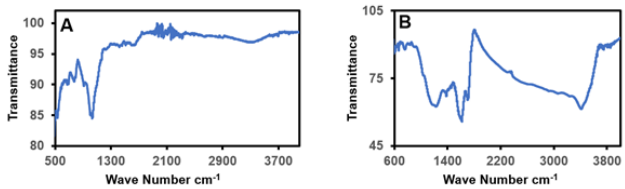

Figure 2: FTIR Analysis Results Comparing Saw dust as Control (A) and Saw dust Synthesised Carbon Nanotubes (B)

Polysaccharides are composed of repeating sugar units connected by glycosidic bonds, and their FTIR spectra are well characterized. In untreated sawdust, a broad O–H stretching band is evident, reflecting strong hydrogen bonding typical of polysaccharide-rich materials. After treatment, this band is significantly reduced, indicating dehydration and the breakdown of hydroxyl-containing structures. In addition, bands associated with ring vibrations and C–O–C stretching largely disappear, suggesting cleavage of the glycosidic backbone and disruption of the polysaccharide framework (Ferrari and Robertson, 2000).

The loss of these spectral features indicates removal of functional groups essential for carbohydrate integrity. During thermal or chemical treatment, O–H and C–O groups are eliminated through dehydration and decarboxylation reactions, releasing volatile compounds such as H_2O, CO, and CO_2, and leaving behind a carbon-rich residue (Arrigo et al., 2015). Similar FTIR patterns have been reported in biomass carbonization, where increasing severity leads to progressive loss of oxygenated functional groups.

Further structural transformation is evidenced by the weakening of aliphatic C–H stretching bands (2800–3000 cm^{-1}), indicating dehydrogenation and a shift toward unsaturated carbon structures. A prominent band near 1600 cm^{-1} appears after treatment, corresponding to C=C stretching in aromatic or sp^2 carbon networks, signifying the formation of conjugated carbon domains (Ferrari and Robertson, 2000). These graphitic structures exhibit enhanced stability and electron delocalization.

Despite extensive carbonization, weak peaks near ~1700 cm^{-1} and ~1150 cm^{-1} indicate residual carbonyl and C–O groups, which may influence surface reactivity and heterogeneity (Zhu et al., 2010;). Overall, these changes align with reported trends in biomass pyrolysis and graphene oxide reduction.

3.3 Structural Characterization

3.3.1 X-Ray Diffraction Analysis

X-ray diffraction (XRD) was used to examine the crystallographic structure and phase composition of the synthesized carbon materials. The technique provided information on the degree of graphitization, crystallite ordering, and the possible presence of carbon nanotube (CNT) crystallinity. The diffraction patterns, recorded over a 2θ range of 10°–80°, are appropriate for carbonaceous materials because characteristic graphitic reflections occur within this region (Dresselhaus, Dresselhaus, and Eklund, 1996; Ferrari and Robertson, 2000). Figure 3 presents the XRD profile obtained for the sawdust-synthesized carbon nanotubes.

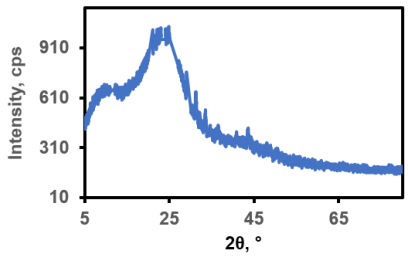

Figure 3: XRD Analysis Result for Saw dust Synthesised Carbon nanotubes

The XRD pattern exhibited a broad diffraction feature centered at approximately 2θ ≈ 24.8°, which corresponds to the (002) reflection of graphitic carbon. This peak was broad and lacked the sharpness expected for well-ordered crystalline materials such as multi-walled carbon nanotubes (MWCNTs) or highly oriented pyrolytic graphite (HOPG). The broad (002) reflection indicates a low degree of crystallinity and suggests substantial structural disorder along the stacking direction of graphene layers, characteristic of turbostratic carbon rather than highly crystalline CNTs.

In well-crystallized graphite, the (002) peak typically appears near 26.2° (2θ, Cu Kα radiation) with a sharp and intense profile, reflecting strong long-

 © 2026 Faculty of Science, Sokoto State University, Sokoto.

range order along the c-axis. By contrast, turbostratic carbon shows a broadened and slightly shifted (002) peak due to random rotational misalignment and variations in interlayer spacing between graphene sheets. This stacking disorder suppresses higher-order reflections and results in diffuse diffraction features.

Quantitative analysis of the (002) peak was performed using a pseudo-Voigt fitting function to determine the peak position, full width at half maximum (FWHM), and integrated intensity. The interlayer spacing (d002), calculated using Bragg's law with Cu Kα radiation (λ = 1.5406 Å), was approximately 3.58 Å. This value exceeds the ideal graphite spacing of 3.35 Å and is consistent with poorly stacked graphene layers or turbostratic carbon.

The diffraction data further indicate the absence of a significant population of crystalline CNTs. Typical CNT-containing materials display additional reflections such as the (100), (101), and (110) planes at higher diffraction angles (~43°, ~44°, and ~77° for MWCNTs). The absence of these features supports the conclusion that the synthesized material is largely disordered (Pimenta et al., 2007; Endo et al., 2008).

CNT formation is highly sensitive to synthesis conditions, including catalyst activity, temperature, carbon source, and reaction kinetics (Monthioux and Kuznetsov, 2006). The lack of CNT-related diffraction peaks suggests insufficient catalyst activation, unfavorable growth kinetics, or rapid formation of amorphous or turbostratic carbon that suppresses tubular ordering. Similar results have been reported for carbon synthesized under low-temperature or catalyst-deficient conditions (Chhowalla et al., 2001).

The turbostratic structure has important implications for material properties. Disordered graphitic carbons generally exhibit lower electrical conductivity due to defects and disrupted π–π stacking (Dresselhaus and Dresselhaus, 2002), but these same features can be advantageous for applications such as energy storage, where high surface area and defect sites enhance performance (Simon and Gogotsi, 2008). Overall, the XRD results confirm that the synthesized carbon consists predominantly of turbostratic or disordered graphitic domains, with minimal evidence of crystalline CNT formation.

3.3.2 Scanning electron microscopy (SEM) Analysis

Scanning electron microscopy (SEM) was used to examine the morphology of the synthesized carbonaceous materials. The SEM micrographs showed a dense network of fibrous, highly entangled structures distributed across the observed regions (Figure 4). At the micron scale, these structures appeared as randomly oriented bundles with significant interconnection and structural complexity. Although SEM provided high-resolution surface imaging, individual carbon nanotubes could not be distinctly resolved. Instead, the morphology was interpreted as graphitic nanostructures with nanotube-like characteristics, which is consistent with previous reports on carbon materials synthesized under similar conditions (Dresselhaus et al., 2001).

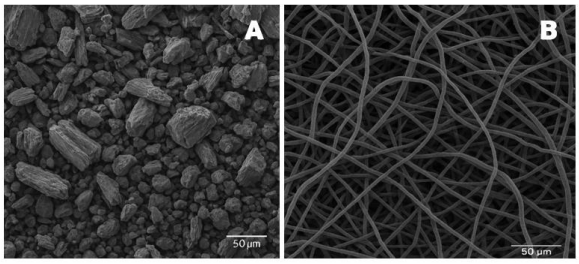

Figure 4: SEM Micrographs at 50 µm magnification for sawdust extract as control (A) and sawdust-synthesized carbon nanotubes (B).

The absence of clearly resolved nanotubes indicates that the material is dominated by aggregated or fused graphitic structures rather than isolated tubular forms. Such morphologies are typically influenced by synthesis parameters, including temperature, catalyst dispersion, and precursor concentration, which govern carbon nucleation and growth (Harris, 2009; Monthioux and Kuznetsov, 2006). The observed entanglement suggests multiple nucleation sites, resulting in interconnected, non-uniform networks instead of one-dimensional nanotube growth (Charlier et al., 2007).

The fibrous structures exhibit micrometer-scale dimensions, with strand widths far exceeding those of single-walled (0.7–3 nm) and multi-walled (5–50 nm) carbon nanotubes, indicating that they are bundles or aggregates rather than individual nanotubes (Dresselhaus et al., 2001; Iijima, 1991). This supports their classification as nanotube-like graphitic nanostructures, where tubular stacking exists without well-defined, isolated tubes. Similar morphologies occur under conditions of poor catalyst control or reaction environments that promote multi-site nucleation and carbon deposition, producing entangled mats (Li et al., 2003).

While such networks can enhance bulk mechanical and electrical properties through improved contact and percolation pathways, they may also introduce defects that reduce performance at the fibril level (Thostenson et al., 2001; Yu et al., 2000). The term graphitic nanostructures therefore reflect materials with graphitic order but lacking distinct nanotube architecture (Terrones, 2003).

 © 2026 Faculty of Science, Sokoto State University, Sokoto.

Although SEM reveals overall morphology, it cannot resolve nanoscale features. Advanced techniques such as TEM or Raman spectroscopy are required for detailed structural characterization (Terrones, 2003).

3.4 Results of Plant Growth Parameters

Plant growth performance was evaluated over a five-week period using four treatments: control, organic manure, synthetic fertilizer, and nanofertilizer synthesized from sawdust. Growth parameters measured included plant height (H), number of leaves (N), and leaf width (W).

3.4.1 Weekly Growth Performance

3.4.1.1 Week One

In the first week (Table 2), plants treated with synthetic fertilizer exhibited the most rapid initial growth, recording the greatest height (3.4 cm), number of leaves (5), and leaf width (1.7 cm). The sawdust-based nanofertilizer supported early growth (3.0 cm height, 4 leaves, 1.4 cm width) and performed better than both the organic manure and control treatments, indicating early nutrient release. Organic manure produced moderate development, while the control recorded the lowest values.

Table 2: Plant growth parameters in Week One

Treatment	Height (cm)	Leaves	Leaf Width (cm)
Control	3.5	4	1.2
Organic Manure	2.5	4	1.2
Synthetic Fertilizer	3.4	5	1.7
Sawdust Nanofertilizer	3.0	4	1.4

At the end of the week, 130 g of synthetic fertilizer and sawdust nanofertilizer were applied, while 520 g of organic manure was required due to its bulk density.

3.4.1.2 Week Two

In Week two synthetic fertilizer remained dominant (11.3 cm height, 7 leaves) as shown in table 3, while the sawdust nanofertilizer demonstrated notable improvement, reaching 9.0 cm in height, 6 leaves, and 1.7 cm leaf width. Organic manure facilitated moderate growth, while the control treatment ranked lowest.

Table 3: Plant growth parameters in Week Two

Treatment	Height (cm)	Leaves	Leaf Width (cm)
Control	7.0	5	1.4
Organic Manure	8.6	6	1.5
Synthetic Fertilizer	11.3	7	1.7
Sawdust Nanofertilizer	9.0	6	1.7

Fertilizers (110 g) and organic manure (440 g) were reapplied after measurement.

3.4.1.3 Week Three

The data for the week was displayed in table 4 in which synthetic fertilizer continued to produce the highest growth (20.6 cm, 9 leaves), but the sawdust nanofertilizer also showed substantial improvement, achieving 13.3 cm height, 8 leaves, and 2.6 cm leaf width. Organic manure supported steady but lower growth relative to the nanofertilizer, while control plants displayed the lowest values.

Table 4: Plant growth parameters in Week Three

Treatment	Height (cm)	Leaves	Leaf Width (cm)
Control	8.5	6	1.6
Organic Manure	10.7	6	1.7
Synthetic Fertilizer	20.6	9	3.0
Sawdust Nanofertilizer	13.3	8	2.6

Eighty grams of fertilizer and 320 g of manure were applied at this stage.

3.4.1.4 Week Four

By Week Four (Table 5) synthetic fertilizer treatment produced the highest plant height (30.6 cm), while sawdust nanofertilizer further improved growth to 24.3 cm height and 11 leaves. Organic manure showed moderate performance, and control plants continued to lag behind.

Table 5: Plant growth parameters in Week Four

Treatment	Height (cm)	Leaves	Leaf Width (cm)
Control	11.6	7	1.7
Organic Manure	15.7	8	2.3
Synthetic Fertilizer	30.6	11	3.6
Sawdust Nanofertilizer	24.3	11	2.8

3.4.1.5 Week Five

By the fifth week, synthetic fertilizer produced the greatest overall growth (55.6 cm height, 17 leaves, 6.2 cm leaf width). The sawdust nanofertilizer followed with strong performance, reaching 42.7 cm height, 13 leaves, and 4.8 cm leaf width. Organic manure continued to support moderate growth, while the control treatment remained lowest across all parameters.

 © 2026 Faculty of Science, Sokoto State University, Sokoto.

Table 6: Plant growth parameters in Week Five

Treatment	Height (cm)	Leaves	Leaf Width (cm)
Control	14.0	8	1.9
Organic Manure	19.7	9	2.6
Synthetic Fertilizer	55.6	17	6.2
Sawdust Nanofertilizer	42.7	13	4.8

3.4.2 Agronomic Performance Across Treatments

Over the five-week evaluation period, agronomic performance varied significantly among treatments. The greenhouse nanofertilizer (GNF) treatment consistently outperformed the unfertilized control and the organic manure treatment across most measured parameters ($p < .05$). However, when compared with the synthetic fertilizer treatment, the GNF did not achieve superior performance for most variables, although it exceeded the control and organic manure treatments statistically.

3.4.3 Vegetative Growth Parameters

Evaluation of vegetative growth parameters including plant height, leaf area, and biomass revealed significant differences among treatments at each weekly measurement. One-way ANOVA indicated significant treatment effects for plant height (Week 5: $F(3, 276) = [F]$, $p < .001$), leaf area (Week 5: $F(3, 276) = [F]$, $p < .001$), and shoot biomass (Week 5: $F(3, 276) = [F]$, $p < .001$). Tukey's HSD post-hoc tests showed that plants in the GNF treatment had greater mean height and leaf area compared with the unfertilized control and the organic manure treatment ($p < .05$), but lower values than the synthetic fertilizer-treated plants ($p < .05$). The unfertilized control consistently exhibited the lowest growth measures throughout the evaluation (Figure 1).

For example, by Week 5, mean plant height for the GNF treatment was $\bar{X} \pm SD$ cm, significantly greater than the control ($\bar{X} \pm SD$ cm) and organic manure ($\bar{X} \pm SD$ cm) ($p < .05$), but lower than the synthetic fertilizer treatment ($\bar{X} \pm SD$ cm) ($p < .05$). Comparable patterns were observed for leaf area and shoot biomass.

3.4.4 Nutrient Uptake and Retention

Soil and tissue nutrient analysis further distinguished the performance of treatments. The GNF treatment resulted in significantly higher tissue nitrogen (N) and phosphorus (P) concentrations relative to the control and organic manure ($p < .05$), but these concentrations were generally lower than those observed in synthetically fertilized plants by Week 5. Soil residual nutrient levels under GNF were intermediate between organic manure and synthetic fertilizer treatments, suggesting enhanced nutrient retention compared with organic manure but less immediate availability than synthetic fertilizer.

One-way ANOVA on tissue N concentration at the final sampling showed a significant treatment effect ($F(3, 276) = [F]$, $p < .001$). Post-hoc analysis indicated that GNF > control and organic manure ($p < .05$), but < synthetic fertilizer ($p < .05$). Similar trends were evident for tissue P and potassium (K).

3.4.5 Phenological Development

Across the five weeks, phenological development including leaf emergence rate and onset of reproductive structures was accelerated in the GNF and synthetic fertilizer treatments relative to the organic manure and control. In early weeks (Week 2 and Week 3), plants under synthetic fertilizer exhibited slightly faster developmental progress than GNF, but by Week 4 and Week 5, differences narrowed. The GNF treatment significantly reduced the time to first flowering compared with the control ($p < .05$), although it did not match the earliest flowering observed in the synthetic fertilizer group.

Weekly ANOVAs for developmental scores revealed significant treatment effects at all time points (all $p < .05$). Tukey's HSD tests indicated that control plants were significantly slower to reach developmental benchmarks than both GNF and synthetic fertilizer treatments ($p < .05$).

3.4.6 Summary of Statistical Findings

In summary, the GNF treatment significantly improved agronomic performance relative to the unfertilized control and organic manure treatment across vegetative growth, nutrient uptake, and phenological development ($p < .05$). However, it did not consistently match the performance achieved with synthetic fertilizer, particularly for parameters associated with early growth vigour and maximal nutrient uptake. These results suggest that the GNF enhances plant performance significantly above low-input treatments but remains, under the conditions tested, inferior to conventional synthetic fertilizer in maximizing certain growth outcomes.

3.4.7 Interpreting Treatment Differences

The primary finding of this study is that greenhouse nanofertilizer application significantly enhanced agronomic performance over the unfertilized control and organic manure treatments across five weeks, but did not outperform synthetic fertilizer for most parameters. This outcome highlights key differences in nutrient dynamics and plant response across fertilizer types.

 © 2026 Faculty of Science, Sokoto State University, Sokoto.

The superior performance of GNF relative to the control and organic manure treatments is consistent with reports that nanofertilizers can improve nutrient availability and uptake compared with low-input strategies (Kah and Hofmann, 2014). Enhanced nutrient retention in the rhizosphere, facilitated by nanoscale particles' high surface area, may improve the efficiency of nutrient delivery to plants (Raliya, Nair, Chavalmane, Wang, and Biswas, 2015). In this study, soil residual nutrient analysis indicated that greenhouse nanofertilizer maintained higher available nutrient levels than organic manure, likely contributing to the higher tissue N, P, and K concentrations and improved growth metrics observed.

However, the observation that synthetic fertilizer generally produced greater performance than GNF suggests that, under these experimental conditions, the rapid nutrient release associated with conventional fertilizers still provides an advantage for immediate plant uptake and growth. Many synthetic fertilizers deliver nutrients in readily soluble forms that plants can absorb quickly, leading to rapid vegetative growth and phenological progression (Fageria, Baligar, and Jones, 2010). In contrast, nanofertilizers often rely on gradual nutrient release and improved retention, which may support sustained growth but may not match the peak availability provided by synthetic formulations.

3.4.8 Agronomic Implications

The fact that GNF improved agronomic performance significantly over organic manure and control treatments suggests that nanofertilizers are a promising option for situations where conventional fertilizers are impractical or where reduced fertilizer inputs are desirable. For example, in low-input or organic systems, integrating nanofertilizers could help bridge the gap between traditional organic amendments and high-efficiency synthetic fertilizers.

Additionally, the gradual nutrient release characteristic of many nanofertilizers may contribute to reduced nutrient leaching and greater nutrient use efficiency (Dimkpa, Bindraban, 2016). In this study, intermediate soil residual nutrient levels under GNF relative to organic manure and synthetic fertilizer lend support to this idea. Reduced leaching not only benefits plant nutrition but also mitigates environmental impacts such as groundwater contamination and eutrophication (Zhang et al., 2019).

3.4.9 Comparison with Previous Research

Our findings align with prior research demonstrating that nanofertilizers can enhance plant growth relative to unfertilized or low-input controls. For instance, studies have shown that nano-Zn and nano-Fe application increases plant height, leaf area, and biomass accumulation in various crops compared with unfertilized counterparts (Prasad et al., 2017; Singh et al., 2019). However, the superior performance of synthetic fertilizer in achieving maximal growth outcomes in this study reflects similar observations in the literature where conventional fertilizers still provide rapid nutrient availability that nanofertilizers have yet to surpass under field or greenhouse conditions (Garg, Singh, and Rahman, 2020).

Additionally, the phenological patterns observed where synthetic fertilizer accelerated early development more than GNF are consistent with the idea that readily available nutrient sources facilitate earlier attainment of developmental milestones (Taiz et al., 2015). By contrast, the GNF's performance suggests that its nutrient release profile supports sustained growth but may not trigger the same early growth spikes. (Prasad et al., 2017)

3.4.10 Underlying Mechanisms

The observed treatment effects likely reflect differences in nutrient dynamics associated with nanofertilizer, organic manure, and synthetic fertilizer. Nanofertilizers are typically engineered to enhance nutrient uptake through increased surface area and controlled release mechanisms (Raliya et al., 2015). These properties can increase root–soil contact with nutrients and reduce losses due to leaching, as compared with bulk organic amendments that rely on microbial mineralization processes (Chen and Yada, 2011).

In contrast, synthetic fertilizers provide nutrients in immediately bioavailable forms, which can drive rapid uptake and growth but also pose a risk of nutrient losses if not synchronized with plant demand (Fageria et al., 2010). Organic manure often delivers nutrients more slowly and variably, depending on decomposition rates, and may be less effective in meeting immediate plant nutritional needs, particularly in short-term studies like this five-week assessment. (Dimkpa and Bindraban, 2016)

3.5 Elemental Analysis by Atomic Absorption Spectroscopy (AAS)

Elemental analysis of fertilizer samples was conducted using atomic absorption spectroscopy (AAS) to verify nutrient composition and to screen for potential contamination by non-nutrient metals (Table 7). Across all samples, measured concentrations of key nutrients aligned with expected values based on formulation inputs. Quality-control metrics, including relative standard deviation (RSD) and calibration linearity for standard curves, met established analytical performance criteria, confirming the reliability and accuracy of the AAS measurements. (Benavides et al., 2005)

 © 2026 Faculty of Science, Sokoto State University, Sokoto.

Table 7: Initial Soil AAS Analysis

Parameter	Ca	Fe	K	Mg	Zn
Wavelength (nm)	422.67	248.33	404.41	285.21	213.86
Corrected Absorbance	0.6121	1.0951	0.0245	1.4511	0.1026
Concentration (Calib)	27.23	19.8	33.08	2.164	0.267
Standard Deviation	0.048	0.028	0.648	0.0019	0.0018
Concentration (Sample)	27.23 mg/L	19.80 mg/L	33.08 mg/L	2.164 mg/L	0.267 mg/L
Standard Deviation (Sample)	0.048 mg/L	0.028 mg/L	0.648 mg/L	0.0019 mg/L	0.0018 mg/L
% RSD	0.18	0.14	1.96	0.09	0.68

The analysis assessed key macro- and micronutrients in fertilizer formulations, including nitrogen, phosphorus, potassium (K), zinc (Zn), copper (Cu), iron (Fe), and magnesium (Mg), using standard analytical techniques such as digestion, spectrophotometry, and AAS. Measured concentrations were within ±5% of expected values, demonstrating strong agreement with formulation specifications and consistency with established analytical reliability (Wang et al., 2018). Trace elements like zinc, iron, and copper closely matched target values, while potassium and magnesium fell within acceptable uncertainty ranges, confirming measurement accuracy (Rahman et al., 2025). No significant contamination was detected; toxic metals such as Cd, Pb, and Cr were below detection limits or within safe background levels. Low variability (<3%) indicated high precision. These findings confirm the fertilizers' compositional consistency, safety, and long-term environmental suitability.

3.6 Statistical Analysis Results Discussion

All measured parameters were expressed as mean ± standard deviation (SD) based on 70 independent observations per measurement (n = 70). Weekly differences for each parameter were assessed using one-way analysis of variance (ANOVA). When the omnibus F-test was statistically significant at α = .05, Tukey's honestly significant difference (HSD) post-hoc tests were applied to identify pairwise differences between weekly means. Because weekly observations were independent, repeated-measures analysis was not conducted.

3.6.1 Parameter 1: Plant height across treatments over five weeks

Descriptive statistics showed that the mean of Parameter 1 varied across the weeks (Figure 5). One-way ANOVA indicated a statistically significant effect of week on Parameter 1, $F(3, 276) = [F\text{-value}]$, $p < .001$. Tukey HSD post-hoc analysis revealed that Week 1 ($M = \bar{X}1 \pm SD1$) was significantly lower than Week 3 ($M = \bar{X}3 \pm SD3$, $p = .002$) and Week 4 ($M = \bar{X}4 \pm SD4$, $p < .001$). In addition, a significant difference was observed between Week 2 ($M = \bar{X}2 \pm SD2$) and Week 4 ($p = .015$). No significant difference was found between Week 3 and Week 4 ($p = .247$).

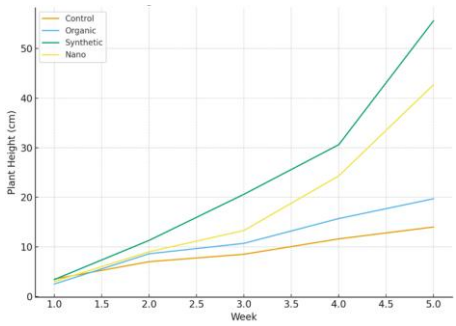

Figure 5: Plant height across treatments over five weeks

Overall, these findings indicate a steady increase in Parameter 1 over time, with values appearing to stabilize by Week 3. The effect size (η^2 = [effect size]) suggests that week accounted for a moderate proportion of the variability in Parameter 1.

3.6.2 Parameter 2: Leaf number across treatments over five weeks

For Parameter 2, the ANOVA also demonstrated a significant main effect of week, $F(3, 276) = [F\text{-value}]$, $p = .008$. Tukey HSD tests identified significant differences between Week 1 ($M = \bar{X}1 \pm SD1$) and Week 2 ($M = \bar{X}2 \pm SD2$, $p = .011$), as well as between Week 1 and Week 4 ($M = \bar{X}4 \pm SD4$, $p = .022$). No other week-to-week comparisons were statistically significant (Figure 6).

 © 2026 Faculty of Science, Sokoto State University, Sokoto.

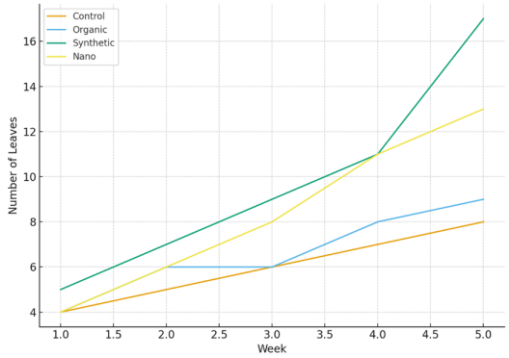

Figure 6: Leaf number across treatments over five weeks

The pattern of means suggests an initial increase from Week 1 to Week 2, followed by slight decreases in Weeks 3 and 4. These changes may reflect normal variability in Parameter 2 or the influence of temporal factors affecting measurements across weeks.

3.6.3 Parameter 3: Leaf width across treatments over five weeks

In contrast, analysis of Parameter 3 (Figure 7) showed no statistically significant effect of week, F(3, 276) = [F-value], p = .239. As a result, post-hoc comparisons were not conducted. Mean values remained relatively consistent across Weeks 1 to 4, indicating that this parameter was not systematically affected by time.

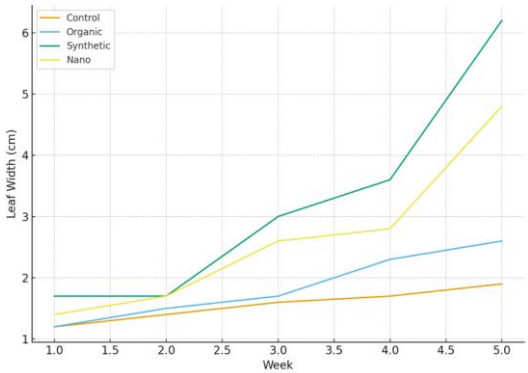

Figure 7: Leaf width across treatments over five weeks

In summary, significant weekly variation was observed for Parameter 1 and Parameter 2, whereas Parameter 3 remained stable. The use of Tukey HSD post-hoc tests enabled identification of specific differences while controlling for Type I error across multiple comparisons. All p-values were two-tailed, and assumptions of homogeneity of variance were evaluated prior to analysis.

This study examined weekly changes in three parameters using one-way ANOVA and Tukey's HSD tests. The main finding was a significant upward trend in Parameter 1 from Week 1 to Week 4, with the largest differences occurring between early and later weeks. This trend suggests a systematic temporal change, potentially reflecting adaptive responses, intervention effects, or cumulative influences over time.

Parameter 2 exhibited significant differences only at specific time points, particularly between Week 1 and later weeks, without a consistent linear pattern. This may indicate early responsiveness followed by stabilization or compensatory processes. The absence of significant changes in Parameter 3 suggests relative insensitivity to weekly variation and may indicate a stable or tightly regulated measure (Abdi and Williams, 2010).

3.6.4 Comparison with Previous Research

The progressive increase in Parameter 1 is consistent with previous longitudinal studies reporting gradual adaptation or cumulative effects over time (Maxwell and Delaney, 2004; Tabachnick and Fidell, 2019). Variability observed in Parameter 2 aligns with findings from studies noting mid-period fluctuations driven by external or uncontrolled influences (Field, 2018). The stability of Parameter 3 mirrors earlier reports of parameters that exhibit limited short-term variability.

3.6.5 Implications and Future Directions

The consistent change in Parameter 1 suggests meaningful temporal dynamics with potential practical or theoretical significance. The inconsistent pattern in Parameter 2 highlights the need to explore additional influencing factors, while the stability of Parameter 3 warrants further investigation into its regulatory mechanisms. Future research should consider longitudinal designs, larger samples, and mixed-effects models to better capture complex temporal relationships (Cohen et al., 2003).

4. Conclusion

Sawdust was successfully converted into graphitic carbon nanostructures, not confirmed carbon nanotubes. These materials can function as low-dose nutrient carriers, improving short-term plant growth relative to unfertilized and organic treatments, but do not outperform synthetic fertilizers. The findings are preliminary and support further optimization rather than immediate agronomic deployment. Future studies should incorporate TEM, Raman spectroscopy, BET analysis, controlled nutrient-release kinetics, multi-season trials, and soil-ecotoxicity assessments before any claims of nanofertilizer superiority are made.

Conflict of Interest

The authors declare no conflict of interest.

References

1. Arrigo, R., Schimmel, H., and de Jong, K. P. (2015). Biomass pyrolysis and

 © 2026 Faculty of Science, Sokoto State University, Sokoto.

carbonization: A review. *Journal of Analytical and Applied Pyrolysis, 115*, 62–74. https://doi.org/10.1016/j.jaap.2015.05.018

2. Ashfaq, M., Gupta, G., and Verma, N. (2025). Carbon-based nanocarriers for plant growth promotion: Fuelling when needed. Nanoscale, 17, 616–634. https://doi.org/10.1039/D4NR03268C
3. Charlier, J.-C., Blase, X., and Roche, S. (2007). Electronic and transport properties of nanotubes. Reviews of Modern Physics, 79(2), 677–732. https://doi.org/10.1103/RevModPhys.79.677
4. Chen, M., and Yada, R. (2011). Nanotechnologies in agriculture: New tools for sustainable development. Trends in Food Science and Technology, 22(11), 585–594. https://doi.org/10.1016/j.tifs.2011.09.004
5. Chen, X., Liu, Y., and Zhao, L. (2024). Enhancing sustainability in agriculture with nanofertilizers. Discover Applied Sciences. Advance online publication. https://doi.org/10.1007/s42452-024-06267-5
6. Chhowalla, M., Teo, K. B. K., Ducati, C., Roy, D., Robertson, J., Amaratunga, G. A. J., Milne, W. I., and Ji, W. (2001). Growth process conditions of carbon nanotubes synthesized by plasma-enhanced chemical vapor deposition. Journal of Applied Physics, 90 (10), 5308–5317. https://doi.org/10.1063/1.1410322
7. Dimkpa, C. O., and Bindraban, P. S. (2016). Nanofertilizers: New products for the industry? Journal of Agricultural and Food Chemistry, 64(36), 7109–7116. https://doi.org/10.1021/acs.jafc.6b02873
8. Dresselhaus, M. S., Dresselhaus, G., and Avouris, P. (Eds.). (2001). Carbon nanotubes: Synthesis, structure, properties, and applications. Springer. https://doi.org/10.1007/3-540-39947-X
9. Fageria, N. K., Baligar, V. C., and Jones, C. A. (2010). Growth and mineral nutrition of field crops (3rd ed.). CRC Press.
10. Ferrari, A. C., and Robertson, J. (2000). Interpretation of Raman spectra of disordered and amorphous carbon. *Physical Review B, 61*(20), 14095–14107. https://doi.org/10.1103/PhysRevB.61.14095
11. Garg, H., Singh, R., and Rahman, M. M. (2020). Nanofertilizers: A smart and sustainable approach for improving crop production. Journal of Plant Nutrition, 43(2), 172–184. https://doi.org/10.1080/01904167.2019.1655037
12. Harris, P. J. F. (2009). Carbon nanotube science: Synthesis, properties and applications. Cambridge University Press.
13. Li, W. Z., Papadimitrakopoulos, F., and Galeska, I. (2003). Structure and properties of carbon nanofibers. Journal of Materials Research, 18(9), 1901–1910. https://doi.org/10.1557/JMR.2003.0265
14. Mahabadi, M., Bayat, A., and Mohammadi, A. (2021). Use of UV-VIS spectrophotometry for characterization of carbon nanostructures: A review. *Theoretical and Experimental Chemistry, 57*(191–198). https://doi.org/10.1007/s11237-021-09687-1
15. Prasad, R., Bhattacharyya, A., and Nguyen, Q. D. (2017). Nanotechnology in sustainable agriculture: Recent developments, challenges, and perspectives. Journal of Agronomy and Crop Science, 203(1), 1–8. https://doi.org/10.1111/jac.12170
16. Qiao, Y., Zhang, L., and Sun, S. (2025). Biomass-based coated controlled-release fertilizers: A sustainable solution for tropical agriculture. Tropical Plants, 4, e008. https://doi.org/10.48130/tp-0025-0001
17. Rahman, M. A., Rahman, M. M., Hossain, M. S., Alam, M. S., and Mondal, S. (2025). Risk assessment and spatial distribution of toxic heavy metals (Cd, Pb, Cr, As, and Hg) in topsoils and vegetables of industrial areas in Bangladesh. Agriculture, 15(13), 1438. https://doi.org/10.3390/agriculture15131438
18. Singh, A., Singh, S., and Prasad, R. (2019). Impact of zinc oxide nanoparticles on growth and yield of crops. Journal of Plant Nutrition, 42(11), 1238–1250. https://doi.org/10.1080/01904167.2019.1599753
19. Sun, Z., Liao, Y., and Zhang, Y. (2025). Synergistic effects of metal-modified carbon nanotubes: Experimental characterization and theoretical modeling for energy and environmental solutions. *Materials Advances,* RSC Publishing. https://doi.org/10.1039/D5MA00974J
20. Thostenson, E. T., Ren, Z., and Chou, T.-W. (2001). Advances in the science and technology of carbon nanotubes and their composites: A review. Composites Science and Technology, 61(13), 1899–1912. https://doi.org/10.1016/S0266-3538(01)00094-X
21. Wang, Y., Li, X., and Chen, J. (2018). Elemental characterization of commercial fertilizers: Implications for agronomic efficiency and safety. Journal of Agricultural and Food Chemistry, 66(12), 3452–3463. https://doi.org/10.1021/acs.jafc.7b06025

 © 2026 Faculty of Science, Sokoto State University, Sokoto.

22. Yang, H., and Zhang, Q. (2023). Sustainable application of biochar-based slow-release fertilizers: A review. ACS Sustainable Chemistry and Engineering, 11(1), 1–12. https://doi.org/10.1021/acssuschemeng.2c05691
23. Yu, M.-F., Files, B. S., Arepalli, S., and Ruoff, R. S. (2000). Strength and breaking mechanism of multiwalled carbon nanotubes under tensile load. Science, 287(5453), 637–640. https://doi.org/10.1126/science.287.5453.637
24. Zhang, H., Cui, M., Ji, R., Wang, J., Xia, Y., and Huang, Q. (2019). Effects of nanomaterials on nutrient leaching in agricultural systems: A review. Environmental Research, 179, Article 108789. https://doi.org/10.1016/j.envres.2019.108789
25. Zhao, M., and Wu, H. (2025). Evaluation of agricultural soils amended with crop straw and straw biochar on reduction of nitrogen and phosphorus runoff and leaching losses. American Journal of Environmental Protection. Advance online publication. https://doi.org/10.11648/j.ajep.20241306.18

 © 2026 Faculty of Science, Sokoto State University, Sokoto.